Journal of the European Ceramic Society 39 (2019) 2365–2373

Contents lists available at ScienceDirect

Journal of the European Ceramic Society

journal homepage: www.elsevier.com/locate/jeurceramsoc

Original Article

Microwave dielectric properties of low firing temperature stable scheelite structured (Ca,Bi)(Mo,V)O_4 solid solution ceramics for LTCC applications

Huan-Huan Guo[a], Di Zhou[a,b,*], Li-Xia Pang[b,c], Ze-Ming Qi[d]

[a] Electronic Materials Research Laboratory, Key Laboratory of the Ministry of Education & International Center for Dielectric Research, School of Electronic and Information Engineering, Xi'an Jiaotong University, Xi'an, 710049, China
[b] Department of Materials Science and Engineering, University of Sheffield, Sheffield S1 3JD, UK
[c] Micro-optoelectronic Systems Laboratories, Xi'an Technological University, Xi'an 710032, Shaanxi, China
[d] National Synchrotron Radiation Laboratory, University of Science and Technology of China, Hefei, Anhui 230029, China

ARTICLE INFO

Keywords:
Scheelite structure
Temperature-stable
LTCC
Microwave dielectric properties

ABSTRACT

In the present work, a systematic study on microwave properties of $Ca_{1-x}Bi_xMo_{1-x}V_xO_4$ ($0.2 \le x \le 0.5$) solid solution ceramics synthesized by using the traditional solid-state reaction method was conducted. A scheelite structured solid solution was formed in the composition range $0.2 \le x \le 0.5$. We successfully prepared a microwave dielectric ceramic $Ca_{0.66}Bi_{0.34}Mo_{0.66}V_{0.34}O_4$ with a temperature coefficient of resonant frequency (TCF) near to zero and a low sintering temperature by using (Bi, V) substituted (Ca, Mo) in $CaMoO_4$ to form a solid solution. The $Ca_{0.66}Bi_{0.34}Mo_{0.66}V_{0.34}O_4$ ceramic can be well sintered at only 870 °C and exhibits good microwave dielectric properties with a permittivity (ε_r) ~21.9, a Qf ~18,150 GHz (at 7.2 GHz) (Q = quality factor = 1/dielectric loss; f = resonant frequency), a TCF ~ + 0.1 ppm/°C. The chemical compatibility with silver indicated that the $Ca_{0.66}Bi_{0.34}Mo_{0.66}V_{0.34}O_4$ ceramic might be a good candidate for the LTCC applications.

1. Introduction

The Low Temperature Co-fired Ceramic (LTCC) technology is a multilayer ceramic manufacturing technology that integrates interconnects, passive components, and packages. LTCC is a leading technology for modern electronic devices fabrication and it is widely used in aerospace, military, communications, medical, automotive electronics and other fields [1–4], with a very broad application market and development prospects. Excellent high frequency characteristics, high density integration, and high reliability make the LTCC an indispensable material for the aerospace and military industries. Furthermore, it is worth mentioning that energy saving, material saving, green, and environmental protection have become an unstoppable trend in the development of electronic components industry. The LTCC also caters to this development demand, which minimizes the environmental pollution caused by raw materials, waste materials and production processes [5–8]. Therefore, the development of microwave dielectric ceramics with excellent performance and lower sintering temperature than the melting point of Ag (961 °C) has currently become one of the most important topics in microwave dielectric materials research.

In recent years, microwave dielectric ceramics with a scheelite structure (ABO_4) have attracted much attention due to its high Qf value and low sintering temperature [9,10]. As an important member of the metal molybdate family with a scheelite crystal structure, $CaMoO_4$ has a wide application potential in various fields, such as solid-state scintillators [11], luminescence material [12], and microwave devices applications [13]. Choi et al. reported that $CaMoO_4$ can be sintered at 1100 °C and exhibits excellent microwave dielectric properties with a permittivity (ε_r) ~ 11.7, a Qf ~ 55,000 GHz (Q = quality factor = 1/dielectric loss; f = resonant frequency), a temperature coefficient of resonant frequency (TCF) ~ −60 ppm/°C [13]. However, temperature coefficient of resonant frequency is the key physical parameter for evaluating the temperature stability of microwave devices. In practical applications, in order to avoid a large drift of the carrier signal of the microwave device as the ambient temperature changes. Therefore, the temperature coefficient of the resonant frequency should be as close as possible to zero. Thus, the high sintering temperature and large negative TCF value limit its application in LTCC technology. Therefore, further studies to reduce its sintering temperature and adjust its TCF to near zero are of great interest. We have noticed that the $BiVO_4$ ceramic with the same scheelite structure have excellent microwave dielectric properties (ε_r = 68, Qf = 8000 GHz, and TCF = − 260 ppm/°C), and it

* Corresponding author at: Electronic Materials Research Laboratory, Key Laboratory of the Ministry of Education & International Center for Dielectric Research, School of Electronic and Information Engineering, Xi'an Jiaotong University, Xi'an, 710049, China.
E-mail address: zhoudi1220@gmail.com (D. Zhou).

https://doi.org/10.1016/j.jeurceramsoc.2019.02.010
Received 25 October 2018; Received in revised form 21 January 2019; Accepted 3 February 2019
Available online 05 February 2019
0955-2219/

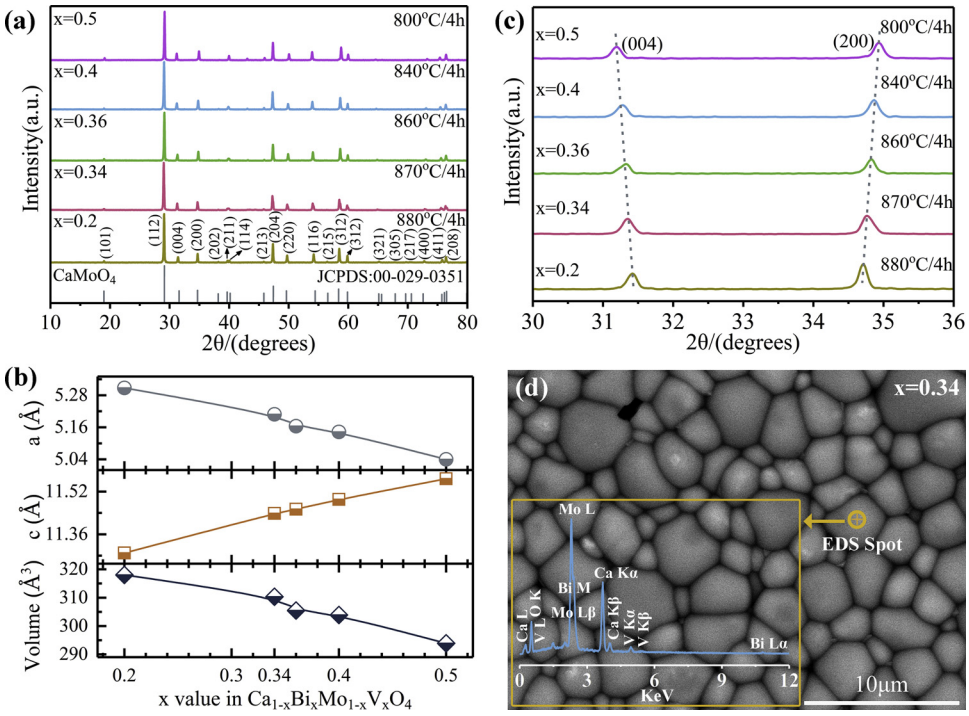

Fig. 1. (a) X-ray diffraction patterns of the $Ca_{1-x}Bi_xMo_{1-x}V_xO_4$ ($0.2 \le x \le 0.5$) ceramics sintered at optimal temperatures. (b) Cell parameters as a function of the x value. (c) The enlarged portion of the $Ca_{1-x}Bi_xMo_{1-x}V_xO_4$ ($0.2 \le x \le 0.5$) XRD patterns ranging from $2\theta = 30\text{-}36^\circ$. (d) Back-scattered electron images of the as-fired surfaces of $Ca_{0.66}Bi_{0.34}Mo_{0.66}V_{0.34}O_4$ ceramic sintered at 870 °C/4 h (insert is the associated Energy dispersive spectra).

is important to point out that its sintering temperature is only 820 °C [14,15]. In addition, the internal stress can be introduced into the monoclinic scheelite-structured $BiVO_4$ ceramic through ion substitution. [16–18] With the increase of ion substitution, the internal stress increases and the crystal structure gradually transforms from monoclinic to tetragonal phase and TCF will become positive. The low sintering temperature, similar ionic radius ($r_{Bi^{3+}} = 1.17$ Å similar to $r_{Ca^{2+}} = 1.12$ Å, $r_{V^{5+}} = 0.355$ Å similar to $r_{Mo^{6+}} = 0.41$ Å), [19] and the common scheelite structure, which usually has wide cation solubility make the $CaMoO_4$ and the $BiVO_4$ are very attractive constituents for the goal of developing LTCC dielectrics.

In this investigation, the $Ca_{1-x}Bi_xMo_{1-x}V_xO_4$ ($0.2 \le x \le 0.5$) solid solution ceramics were synthesized by solid-state reaction method. The structural evolution, sintering behaviors, microstructures, microwave dielectric properties, infrared (IR) reflectivity spectra, Raman, chemical compatibility with Ag, and the relation between structure and microwave dielectric properties were investigated in detail.

2. Experimental section

Samples of the $Ca_{1-x}Bi_xMo_{1-x}V_xO_4$ ($0.2 \le x \le 0.5$) were synthesized by using the conventional solid-state reaction method, and the raw materials were $CaCO_3$ (99.8%), Bi_2O_3 (99%), MoO_3 (99.95%) and V_2O_5 (99%). Then the mixed powders were ball-milled in a nylon jar with zirconia balls for 4 h using ethanol as a medium. The mixtures were calcined at 650 °C for 4 h in air. After being crushed, the calcined powders were re-milled with ethanol for 4 h using a planetary mill, dried, and the as-dried powders were ground with 5 wt.% polyvinyl alcohol (PVA) binder addition and uniaxially pressed into several pellets (10 mm in diameter and 4–5 mm in height) under a pressure of 100 MPa. Samples were sintered in the temperature range 780–880 °C for 4 h. In order to study the chemical compatibility of the scheelite solid solution compound with Ag electrode, 20 wt.% Ag powders was mixed with the temperature-stable $Ca_{0.66}Bi_{0.34}Mo_{0.66}V_{0.34}O_4$ ceramic powders and co-fired at 870 °C for 2 h.

The samples were investigated using room-temperature X-ray diffraction (XRD)with Cu Kα radiation (Rigaku D/MAX-2400 X-ray diffractometry, Tokyo, Japan). The microstructures and energy-dispersive spectroscopy (EDS) of the sintered samples was observed by electron scanning microscopy (SEM; Quanta 250, FEI). The mean grain size was calculated from each SEM image of the $Ca_{1-x}Bi_xMo_{1-x}V_xO_4$ ($0.2 \le x \le 0.5$) sample using image analysis software (Nano Measurer 1.2) [20]. The high-resolution transmission electron microscopy (HRTEM) and selected area electron diffraction (SAED) patterns measurements were conducted on a JEM-2100 at an accelerating voltage of 200 kV. The Raman spectra were performed with a Laser Raman Spectrometer. The room temperature infrared reflectivity spectra were measured using a Bruker IFS 66v FTIR spectrometer on Infrared beamline station (U4) at National Synchrotron Radiation Lab (NSRL), China. The X-ray photoelectron spectroscopy (XPS) analysis was measured for the $Ca_{0.66}Bi_{0.34}Mo_{0.66}V_{0.34}O_4$ by a Thermo Fisher ESCALAB Xi^+ with a monochromatic Al K_α radiation source. The microwave dielectric properties were measured using a network analyzer (8720ES, Agilent, Palo Alto, CA) and a temperature chamber (Delta 9023, Delta Design, Poway, CA). The temperature coefficient of resonant frequency (TCF) was measured in the temperature range from 25 °C ~ 85 °C. The TCF values were calculated by the following equation:

$$TCF(\tau_f) = \frac{f_T - f_{T_0}}{f_{T_0} \times (T - T_0)} \times 10^6 \quad (1)$$

where, f_T and f_{T_0} represent resonant frequencies at temperatures T and T_0, respectively.

3. Results and discussion

X-ray diffraction (XRD) patterns of the $Ca_{1-x}Bi_xMo_{1-x}V_xO_4$ ($0.2 \le x \le 0.5$) ceramics sintered at their optimal temperatures are presented in Fig. 1a. All compositions were found to crystallize in a scheelite structure with no second phase observed from the XRD results, indicating that the tetragonal scheelite structure (space group $I4_1/a$) is stable for the $Ca_{1-x}Bi_xMo_{1-x}V_xO_4$ ($0.2 \le x \le 0.5$). Due to the difference in ionic radius ($r_{Bi^{3+}} = 1.17$ Å $> r_{Ca^{2+}} = 1.12$ Å, CN = 8; $r_{V^{5+}} = 0.355$ Å $< r_{Mo^{6+}} = 0.41$ Å, CN = 4) [19], a slight change in lattice parameters will occur as the amount of substitution of (Bi,V) increases. The lattice parameters of the $Ca_{1-x}Bi_xMo_{1-x}V_xO_4$ ($0.2 \le x \le 0.5$) ceramics were calculated by the least squares method using Jade software [21]. To

observe the changes in lattice parameters clearly, cell parameters of the $Ca_{1-x}Bi_xMo_{1-x}V_xO_4$ ($0.2 \le x \le 0.5$) ceramics as a function of x value are shown in Fig. 1b. The lattice parameters *a* decreased from 5.308 to 5.040 Å while the lattice parameters *c* increased from 11.290 to 11.568 Å with the increase of x, along with a decrease in the cell volume from 318.04 to 293.89 $Å^3$. In order to show the changes of the diffraction peaks clearly, the enlarged portion of the XRD patterns from 30° to 36° are presented in Fig. 1c. With the increase of substitution content, the (004) diffraction peak shifted towards lower angle direction while the (200) diffraction peak shifted towards higher angle direction. It is commensurate with the enlargement of *c* axis and contraction of *a* axis, respectively. Because for the tetragonal system, the following equation can be derived from the Bragg's equation ($2d\sin\theta = \lambda$) and d-spacings formula ($1/d^2 = (h^2+k^2)/a^2 + l^2/c^2$):

$$sin^2\theta = \frac{\lambda^2}{4a^2}(h^2 + k^2) + \frac{\lambda^2}{4c^2}l^2 \quad (2)$$

According to the above formula, the θ of the (200) diffraction peak is inversely proportional to the lattice parameter *a*, and the θ of the (004) diffraction peak is inversely proportional to the lattice parameter *c*. Therefore, the θ of the (200) diffraction peak increased as the lattice parameter *a* decreased, namely, the (200) diffraction peak position shifted toward higher angle direction. The θ of the (004) diffraction peak decreased as the lattice parameter *c* increased, namely, the (004) diffraction peak position shifted toward lower angle direction. The regular shift of the XRD peaks in Fig. 1c and the changes of the lattice parameters in Fig. 1b further indicate the formation of solid solution in the $Ca_{1-x}Bi_xMo_{1-x}V_xO_4$ ($0.2 \le x \le 0.5$) ceramics. This is consistent with the observation from the back-scattered electron images (BEI) and energy dispersive spectra (EDS) analysis of as-fired surfaces of the $Ca_{0.66}Bi_{0.34}Mo_{0.66}V_{0.34}O_4$ ceramic sintered at 870 °C as shown in Fig. 1d. It can be seen that there is only one kind of grain, combined with the analysis results of EDS, further indicating that a solid solution is formed in the $Ca_{0.66}Bi_{0.34}Mo_{0.66}V_{0.34}O_4$ ceramic.

The scanning electron microscopy (SEM) analysis was carried out to study the surface micro-morphology of the $Ca_{1-x}Bi_xMo_{1-x}V_xO_4$ ($0.2 \le x \le 0.5$) ceramics. Fig. 2a–c shows the SEM images (only focus on those that show differences) of the samples sintered at optimal temperatures. It can be seen that all the ceramics exhibit dense microstructures with almost no pores and a relatively flat surface. Fig. 2d shows the mean grain size of the $Ca_{1-x}Bi_xMo_{1-x}V_xO_4$ ($0.2 \le x \le 0.5$) ceramics sintered at optimal temperatures as a function of x value. It can be seen that the mean grain size increased from 2.3 to 3.4 μm with increasing x value. In addition, the sintering temperatures of pure $CaMoO_4$ and $BiVO_4$ ceramics are 1100 °C and 820 °C, respectively [13,15]. However, optimal sintering temperatures of the $Ca_{1-x}Bi_xMo_{1-x}V_xO_4$ ($0.2 \le x \le 0.5$) ceramics are in range 800–880 °C. The reason might be that Bi^{3+} and V^{5+} ions enter the lattice of $CaMoO_4$ to form a solid solution, and the difference in ionic radius ($r_{Bi^{3+}} = 1.17$ Å > $r_{Ca^{2+}} = 1.12$ Å, CN = 8; $r_{V^{5+}} = 0.355$ Å < $r_{Mo^{6+}} = 0.41$ Å, CN = 4) [19] cause a slight lattice distortion of the $CaMoO_4$ phase. These lattice defects would increase the internal energy of the crystal, activate the crystal lattice, and also accelerate the mass mobility, so that the densification of (Ca, Bi)(Mo, V)O_4 ceramics occur at lower temperatures, thereby reducing the optimal sintering temperatures of (Ca, Bi)(Mo, V)O_4 solid solutions. [22–24] Therefore, it is clear that the formation of solid solution can effectively reduce the sintering temperatures of ceramic samples and similar phenomena can be observed in many other solid solution ceramic systems, such as $x(Ag_{0.5}Bi_{0.5})MoO_4$-(1-x)$BiVO_4$, (1-x)$BiVO_4$-x$La_{2/3}MoO_4$ and $(Na_xAg_{2-x})MoO_4$ etc. [15,25,26]

The bulk density, theoretical density and microwave dielectric properties ε_r, Qf and TCF of the $Ca_{1-x}Bi_xMo_{1-x}V_xO_4$ ($0.2 \le x \le 0.5$) ceramics sintered at optimal temperatures as a function of x value are shown in Fig. 3. It can be seen that the bulk density increases linearly with the increase of x. To make clear the changes of density with composition, we also calculated the theoretical density of the different compositions of the $Ca_{1-x}Bi_xMo_{1-x}V_xO_4$ ($0.2 \le x \le 0.5$) solid solution ceramics according to the theoretical density formula ($\rho_{theo} = \frac{W}{V} = \frac{\sum_{i=1}^{n} W_i}{V}$), where, *W* is the unit cell weight of solid solution, *i* is the atom contained in the unit cell, n is the number of species of atoms contained in the unit cell, *V* is the unit cell volume of the solid solution. The calculated theoretical density as a function of x value are shown in Fig. 3a. It can be seen that the theoretical density also increases linearly with the increase of x, which could be ascribed to the theoretical density of $BiVO_4$ (6.98 g/cm^3) [27] is much larger than that of $CaMoO_4$ (4.25 g/cm^3) [28]. Therefore, the density is gradually increased as the $BiVO_4$ content increases in the $Ca_{1-x}Bi_xMo_{1-x}V_xO_4$ ($0.2 \le x \le 0.5$) solid solution. As shown in Fig. 3b, the ε_r of samples increased linearly from 15.1 to 34.5 as the x value increases from 0.2 to 0.5. The variation in polarizabilities (α_{the}) value versus x value presented similar behavior to that of permittivity, suggesting that the change of permittivity can be explained well by Shannon's additive rule. [29] Shannon suggested that polarizabilities of oxides may be estimated by summing the polarizabilities of constituent ions [29,30]. The polarizabilities α_x of $Ca_{1-x}Bi_xMo_{1-x}V_xO_4$ could be calculated as follows:

$$\alpha_x = (1-x) \times (\alpha_{Ca^{2+}} + \alpha_{Mo^{6+}}) + x \times (\alpha_{Bi^{3+}} + \alpha_{V^{5+}}) + 4\alpha_{O^{2-}} \quad (3)$$

where $\alpha_{Ca^{2+}}$, $\alpha_{Mo^{6+}}$, $\alpha_{Bi^{3+}}$, $\alpha_{V^{5+}}$ and $\alpha_{O^{2-}}$ are the polarizabilities of Ca^{2+}, Bi^{3+}, Mo^{6+}, and V^{5+}, respectively [13,30]. The permittivity can be calculated by the following equation:

$$\varepsilon_{th} = \frac{3V_m + 8\pi\alpha_x}{3V_m - 4\pi\alpha_x} \quad (4)$$

where, V_m is the cell volume, α_x is the sum of ionic polarizability of individual ions. With the increase of substitution content, the increase in permittivity is due to the increase of ionic polarizability coupled with the contraction of cell volume according to the Eq. (4). The ε_{th} of samples increased linearly from 12.3 to 27.9 as the x value increases from 0.2 to 0.5, which is close to the measured dielectric constant. This result indicates that the variation of the dielectric constant with solid solution composition can be well explained by the Shannon's additive rule. Fig. 3(c) shows that the Qf values of the $Ca_{1-x}Bi_xMo_{1-x}V_xO_4$ ceramics decreased with increasing x value. At microwave region, the relationship between Qf value and relative permittivity can be obtained as following:

$$Q \times f \approx \frac{(ze)^2/mV\varepsilon_0}{2\pi\gamma \times (\varepsilon'(\omega) - \varepsilon(\infty))} \quad (5)$$

where *Q* is the quality factor, *f* is the frequency, *z* is the equivalent electric charge number, *e* is the electric charge for an electron, *m* is the equivalent atom weight, *V* is the unit volume, ε_0 is the permittivity, γ is the damping parameter, $\varepsilon'(\omega)$ is the complex permittivity and $\varepsilon(\infty)$ is the electronic part of the static permittivity. The above relation was successfully used to explain the reciprocal relationship between the ε_r and Qf in scheelite solid solutions [31]. It shows that Qf has inverse relation to ε_r, so the Qf values decreased with the increase of the components. It is assumed that the intrinsic microwave dielectric loss is mainly dominated by low frequency modes corresponding to Ca/Bi–Mo/VO4 vibrations. Bi^{3+} (6.12 $Å^3$) has a polarizability larger than Ca^{2+} (3.16 $Å^3$) while V^{5+} (2.92 $Å^3$) has a smaller polarizability than Mo^{6+} (3.28 $Å^3$). However, considering that $\triangle\ \alpha_{Bi^{3+}} - \alpha_{Ca^{2+}}$ is much larger than $\triangle\ \alpha_{Mo^{6+}} - \alpha_{V^{5+}}$, the main contribution should come from Bi^{3+} instead of Ca^{2+}. From $\alpha_{Bi^{3+}} > \alpha_{Ca^{2+}}$ it can be inferred that the contribution to microwave dielectric constant from Bi^{3+} polarization is larger than that of Ca^{2+} and the oscillation of Bi^{3+} is also stronger than that of Ca^{2+} in the scheelite structure. Therefore, the substitution of Bi^{3+} decreases the Qf value of the $Ca_{1-x}Bi_xMo_{1-x}V_xO_4$ ceramics. As shown in Fig. 3d, the TCF value shifts from -44.9 ppm/°C to + 71.6 ppm/ °C as x value increases from 0.2 to 0.5. In general, $BiVO_4$ material has three different structures: monoclinic scheelite, tetragonal zircon

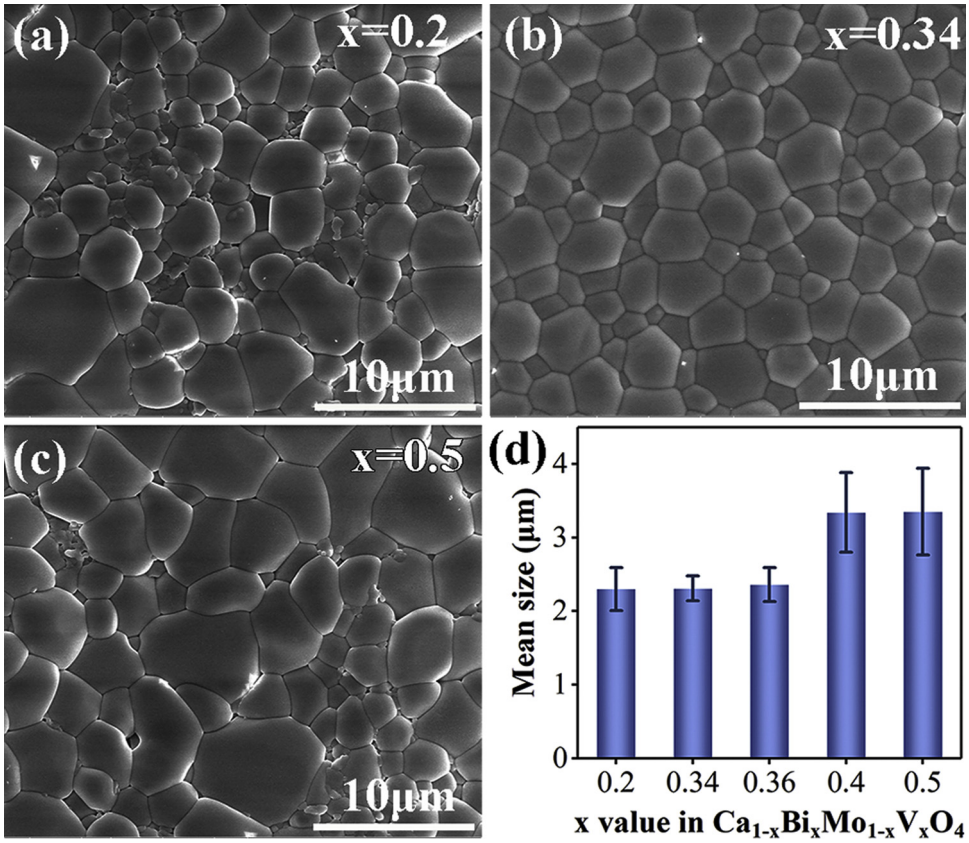

Fig. 2. (a–c) SEM images of the $Ca_{1-x}Bi_xMo_{1-x}V_xO_4$ ($0.2 \le x \le 0.5$) ceramics sintered at optimal temperatures. (d) The mean grain size of the $Ca_{1-x}Bi_xMo_{1-x}V_xO_4$ ($0.2 \le x \le 0.5$) ceramics sintered at optimal temperatures as a function of x value.

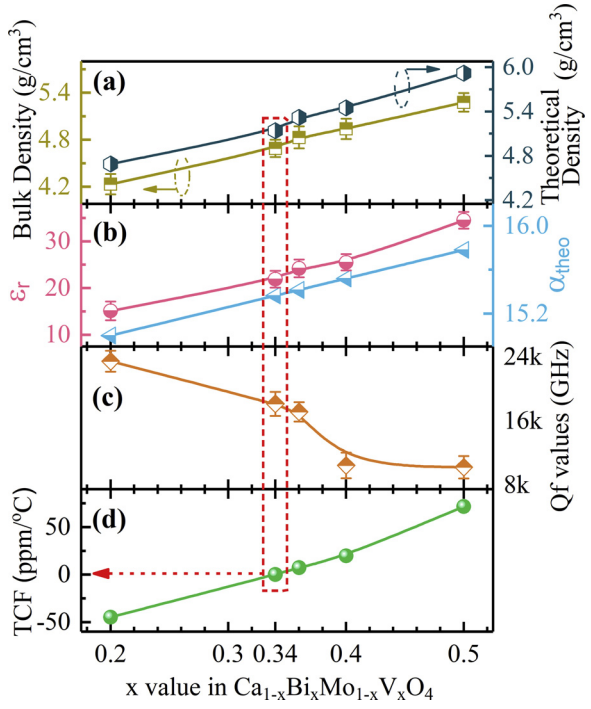

Fig. 3. The bulk density, theoretical density (a), polarizabilities (b) and microwave dielectric properties ε_r (b), Qf (c) and TCF (d) of the $Ca_{1-x}Bi_xMo_{1-x}V_xO_4$ ($0.2 \le x \le 0.5$) ceramics sintered at optimal temperatures as a function of x value.

and tetragonal scheelite. The $BiVO_4$ ceramics synthesized via solid-state reaction method are usually crystallized in a monoclinic scheelite structure. The TCF of $BiVO_4$ with monoclinic scheelite structure is −260 ppm/°C [14,15]. The monoclinic scheelite $BiVO_4$ is ferroelastic at room temperature and reversibly transforms to paraeleastic $BiVO_4$ with a standard tetragonal scheelite structure (space group $I4_1/a$) under high temperature (255 °C) [32]. Besides, according to Hazen et al.'s work, this phase transition can also occur through stress induction [17]. In our previous work, the $(Li_{1/2}Bi_{1/2})^{2+}$ and $(Na_{1/2}Bi_{1/2})^{2+}$ complex ions were introduced into the A site of $BiVO_4$ by ion substitution, and the Mo^{6+} ion was introduced into the B site, and a large internal stress was successfully introduced into the monoclinic scheelite structure. With the increase of the amount of ion substitution, the internal stress gradually increases, causing the lattice parameters to change, then the lattice structure gradually changes from a monoclinic phase to a tetragonal phase. Therefore, the ferroelastic–paraelastic phase transition temperature was shifted from 255 °C to near room temperature, and the TCF value becomes positive [16,18]. This is because the TCF is usually defined as follows:

$$TCF = -\left(\frac{1}{2}\tau_\varepsilon + \alpha_l\right) \tag{6}$$

where τ_ε is the temperature coefficient of dielectric constant and α_l is the thermal expansion coefficient. Generally, the α_l of microwave dielectric is relatively small (< + 20 ppm/ °C). Hence, the TCF value mainly depends on τ_ε. According to our previous work, in the $[(Li_{0.5}Bi_{0.5})_xBi_{1-x}][Mo_xV_{1-x}]O_4$ [16] and $(Na_{0.5x}Bi_{1-0.5x})(Mo_xV_{1-x})O_4$ [18] system, When the materials belong to ferroelastic–monoclinic phase, the relative permittivity increases sharply with temperature ranging from 25 to 85 °C. This determines that it has a large positive temperature coefficient of dielectric permittivity (τ_ε), which means a large negative TCF value. However, when the materials belong to

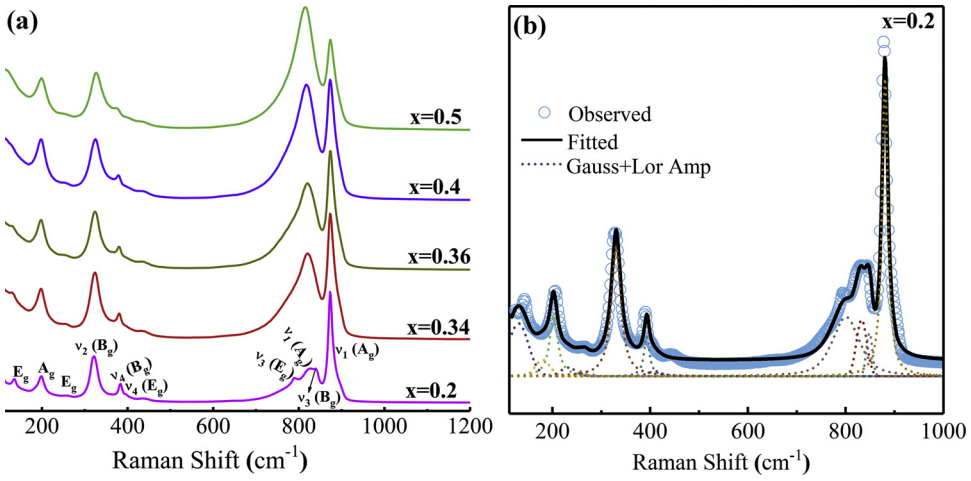

Fig. 4. (a) Raman spectra of $Ca_{1-x}Bi_xMo_{1-x}V_xO_4$ ($0.2 \le x \le 0.5$) ceramics sintered at optimal temperatures as a function of the x value. (b) The experimental (circle) and calculated (black solid line) Raman spectra of $Ca_{0.8}Bi_{0.2}Mo_{0.8}V_{0.2}O_4$ ceramics sintered at optimal temperatures. (The short dot lines represent the Gaussian-Lorentzian fitting results).

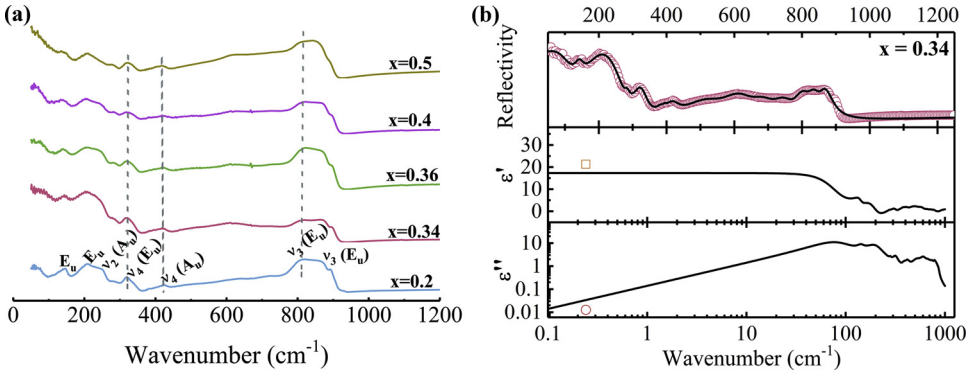

Fig. 5. (a) Far-infrared reflectivity of $Ca_{1-x}Bi_xMo_{1-x}V_xO_4$ ($0.2 \le x \le 0.5$) ceramics. (b) Measured and calculated infrared reflectivity spectra (solid line for fitting values and circle for measured values) and fitted complex dielectric spectra of $Ca_{0.66}Bi_{0.34}Mo_{0.66}V_{0.34}O_4$ ceramic (square and circles are experimental in microwave region).

Table 1
Phonon parameters obtained from the fitting of the infrared reflectivity spectra of $Ca_{0.66}Bi_{0.34}Mo_{0.66}V_{0.34}O_4$ ceramic.

Mode	ω_{oj}	ω_{pj}	γ_j	$\Delta\varepsilon_j$
1	87.11	280.65	96.39	10.40
2	142.38	106.86	27.98	0.56
3	197.49	350.16	90.94	3.14
4	281.35	41.57	15.46	0.02
5	317.61	145.03	42.40	0.21
6	383.08	49.55	23.02	0.02
7	395.00	19.88	7.29	0.01
8	417.82	142.69	51.89	0.12
9	518.40	294.69	128.40	0.32
10	605.27	339.99	111.38	0.32
11	679.28	233.88	91.82	0.12
12	738.05	219.51	75.14	0.09
13	791.39	215.22	55.10	0.07
14	826.64	130.86	43.57	0.03
15	857.10	101.72	36.96	0.01
$CBMV_{0.34}$	$\varepsilon_\infty = 1.86$		$\varepsilon_0 = 17.28$	

paraelastic–tetragonal phase, the relative permittivity decreases sharply with temperature ranging from 25 to 85 °C. This determines that it has a large negative temperature coefficient of dielectric permittivity (τ_ε), which means a positive TCF value. Therefore, the phase transformation from monoclinic to tetragonal structure determines the sign of the TCF value, namely, the TCF value becomes positive. In our previous work, we found that the ferroelastic-paraelastic phase transition could be exist in many systems such as $[(Li_{0.5}Bi_{0.5})_xBi_{1-x}][Mo_xV_{1-x}]O_4$, $(Na_{0.5x}Bi_{1-0.5x})(Mo_xV_{1-x})O_4$ and $(1-x)BiVO_4$–$x(Ag_{0.5}Bi_{0.5})MoO_4$ [16,18,25]. For $[(Li_{0.5}Bi_{0.5})_xBi_{1-x}][Mo_xV_{1-x}]O_4$, $(Na_{0.5x}Bi_{1-0.5x})(Mo_xV_{1-x})O_4$ and $(1-x)BiVO_4$–$x(Ag_{0.5}Bi_{0.5})MoO_4$ systems, the phase transition point occurs at x = 0.098, x = 0.1, and x = 0.1, respectively. In addition, in this wok, both end members (TCF_{CaMoO4} = -60 ppm/°C, TCF_{BiVO4} = -260 ppm/°C) in the $Ca_{1-x}Bi_xMo_{1-x}V_xO_4$ system have negative TCF. However, a near-zero TCF value appears at x = 0.34. Therefore, it was deduced that there should be a phase transition in the range of $0.5 < x < 1$ of the $Ca_{1-x}Bi_xMo_{1-x}V_xO_4$ system, leading the TCF value of $BiVO_4$ shifted from negative to positive, thereby adjusting the negative TCF value of $CaMoO_4$ to near zero. The phase transition in $Ca_{1-x}Bi_xMo_{1-x}V_xO_4$ ($0.5 < x < 1$) solid solutions will be studied in more detail in our future work. It is important to note that a temperature-stable microwave dielectric ceramic can be obtained at x = 0.34, indicating that the substitution of (Bi, V) for (Ca, Mo) in $CaMoO_4$ is an effective method to adjust TCF to near zero. High performance of microwave dielectric properties can be obtained in the $Ca_{0.66}Bi_{0.34}Mo_{0.66}V_{0.34}O_4$ ceramic sintered at 870 °C for 4 h, with a ε_r ~21.9, a Qf ~18,150 GHz (at 7.2 GHz) and a TCF ~ + 0.1 ppm/°C.

In order to further understand the crystal structure of $Ca_{1-x}Bi_xMo_{1-x}V_xO_4$ ($0.2 \le x \le 0.5$), Raman spectroscopic investigation was also conducted. Pure $CaMoO_4$ belongs to a tetragonal crystal structure (space group: $I4_1/a$) with a point group C_{4h} (4/m). The Ca ions are at S_4 sites, as are the Mo's, and the oxygen ions are at C_1 sites. Theoretical group analysis gives an irreducible representation of the vibrational modes as follow :

$$\Gamma = 3A_g + 5A_u + 5B_g + 3B_u + 5E_g + 5E_u \quad (7)$$

The $3A_g$, $5B_g$, $5E_g$ modes are the Raman-active optical modes, whereas the $5A_u$, $3B_u$ and $5E_u$ modes are infrared-active modes. In order to observe the lattice vibrational modes, the Raman spectra of $Ca_{0.8}Bi_{0.2}Mo_{0.8}V_{0.2}O_4$ was fitted by the standard Gaussian-Lorentzian model, then the specific position information of the peaks can be obtained. The fitted Raman spectra are plotted in Fig. 4b as black solid lines. As seen from Fig. 4a, the peaks at 136.0 cm^{-1} (E_g), 198.5 cm^{-1} (A_g) and 258.2 cm^{-1} (E_g) belong to the external modes, and peaks at

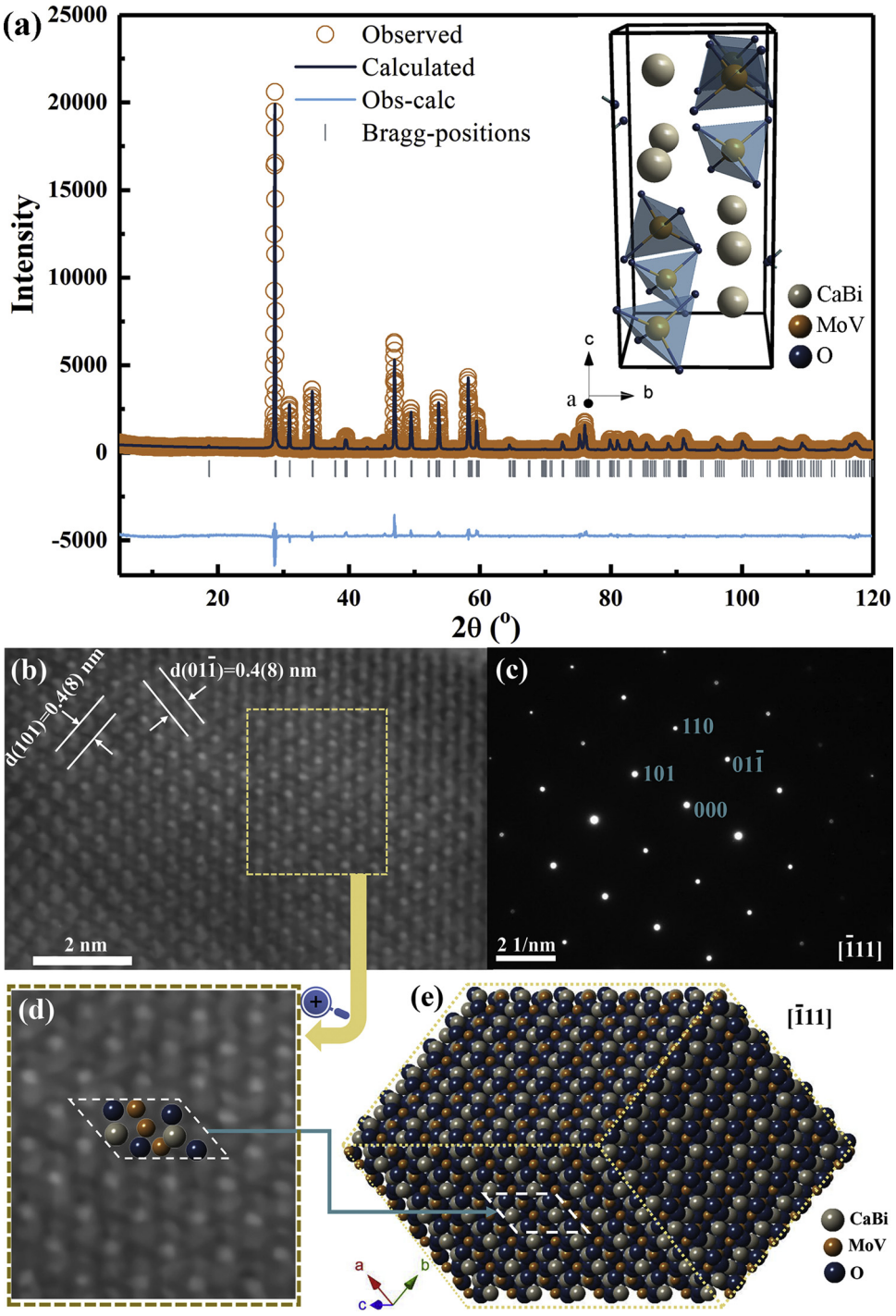

Fig. 6. (a) The experimental (circle) and calculated (line) X-ray powder diffraction profiles for $CBMV_{0.34}$ sample sintered at 870 °C (The short vertical lines below the patterns mark the positions of Bragg reflections. The bottom continuous line is the difference between the observed and calculated intensity.). Insets is the schematic crystal structure of$CBMV_{0.34}$. (b, c, e) HRTEM image, SAED pattern and schematic of crystal structure of $CBMV_{0.34}$viewed along the [$\bar{1}$11] zone axis. (d) The enlarged part of HRTEM image.

320.6 cm^{-1} (B_g), 384.6 cm^{-1} (B_g), 395.0 cm^{-1} (E_g), 789.0 cm^{-1} (E_g), 826.7 cm^{-1} (B_g), 838.5 cm^{-1} (B_g) and 873.2 cm^{-1} (A_g) belong to the internal modes. Each vibration mode is in good agreement with the results reported in the literature [33]. While it is noteworthy that as the increases of x, the intensity of peak at 826.7 cm^{-1} increases gradually, while the intensity of peak at 873.2 cm^{-1} decreases. It is due to that the Raman spectrum of the scheelite ABO_4 structure crystals mainly reflect the structure of the BO_4 tetrahedrons in the scheelite crystals. In the $Ca_{1-x}Bi_xMo_{1-x}V_xO_4$ solid solution, peaks at 826.7 cm^{-1} and 873.2 cm^{-1} represent the anti-symmetric ν_3 stretching mode in the [VO4] tetrahedron and the ν_1 stretching mode in the [MoO4] tetrahedron, respectively. Therefore, as the amount of V substitution increases, the peak at 826.7 cm^{-1} becomes stronger, and the peak at 873.2 cm^{-1} becomes weaker.

Far-infrared reflectivity is an effective method to analyse intrinsic dielectric properties of microwave ceramics. As discussed above, there are thirteen infrared-active modes including $5A_u$, $3B_u$ and $5E_u$ modes. As seen from Fig. 5a, the peaks located at 248.3 cm^{-1} (ν_2-A_u),

Table 2
Refned atomic fractional coordinates from XRD data of the $Ca_{0.66}Bi_{0.34}Mo_{0.66}V_{0.34}O_4$ ceramic and the cell parameters are a = b = 5.2052 Å, c = 11.5470 Å with a space group $I4_1/a$ (No. 88).

Atom	Wyckoff position	Occ.	x	y	z	Biso
Ca	4b	0.165	0.00000	0.25000	0.62500	0.191
Bi	4b	0.085	0.00000	0.25000	0.62500	0.191
V	4a	0.085	0.00000	0.25000	0.12500	0.120
Mo	4a	0.165	0.00000	0.25000	0.12500	0.120
O	16f	1.000	0.15419	−0.01452	0.21038	1.303

318.7 cm^{-1} (ν_4-E_u), 423.6 cm^{-1} (ν_4-A_u), 804.0 cm^{-1} (ν_3-E_u) and 870.4 cm^{-1} (ν_3-E_u) belong to the internal modes, and two external modes located at 143 cm^{-1} (E_u) and 206.7 (E_u) cm^{-1}. All the vibration mode consist with the results reported by Porto [33]. It can be observed that the original ν_3 vibration peaks at 804 cm^{-1} and the external modes vibration peaks become weak as x value increase. In addition, there is only a slight change in ν_4 mode. This may be due to the [MoO_4] tetrahedra distortion caused by (Bi, V) substitution of (Ca, Mo), thereby affecting the position and intensity of the internal mode peaks. Since the microwave dielectric ceramic with TCF of + 0.1 ppm/°C was obtained at x = 0.34, the infrared reflectivity spectra of the $Ca_{0.66}Bi_{0.34}Mo_{0.66}V_{0.34}O_4$ ($CBMV_{0.34}$) ceramic were analyzed using a classical harmonic oscillator model:

$$\varepsilon^*(\omega) - \varepsilon(\infty) = \sum_{j=1}^{n} \frac{(z_j e)^2/m_j V_j \varepsilon_0}{\omega_{Tj}^2 - \omega^2 - j\gamma_j\omega} \tag{8}$$

where, zj is the equivalent price of the j^{th} vibration mode, mj is the equivalent mass of the j^{th} vibrational mode, Vj is the equivalent unit volume of the j^{th} vibrational mode, γj is the damping coefficient of the j^{th} vibrational mode, ω_{Tj} ω_{Tj} is the angular frequency of the transverse optical modes of the *j*th mode of vibration, and n is the number of transverse phonon modes. The relation between complex reflectivity R (ω) and dielectric constant can be written as follows:

$$R(\omega) = \left| \frac{1 - \sqrt{\varepsilon^*(\omega)}}{1 + \sqrt{\varepsilon^*(\omega)}} \right|^2 \tag{9}$$

The fitted infrared reflectivity values and the complex permittivities are shown in Fig. 5b, and the related parameters are listed in Table 1. The calculated permittivity value of 17.3 was obtained according to the fitting result, which is a little smaller than the measured value ~21.9. The optical dielectric constants from the infrared spectra of the $CBMV_{0.34}$ ceramic is about 1.86, which is only 10.8% of the total polarizability contribution at microwave frequencies, indicating that the main polarization contributions to permittivity of microwave dielectric ceramics come from ionic polarization rather than electronic, which is quite popular in high k microwave dielectric ceramics.

As a result, the TCF value of $CaMoO_4$ can be effectively adjusted to zero by replacing (Ca, Mo) by (Bi, V), and a temperature stable microwave dielectric ceramic was obtained at x = 0.34. Therefore, it is necessary to study the $CBMV_{0.34}$ in more detail. In order to investigate the crystal structure details of $CBMV_{0.34}$ ceramic, refinements were performed based on XRD data recorded on the powders. The refinement confirmed that $CBMV_{0.34}$ adopts a tetragonal structure with a space group $I4_1/a$ (No. 88). Measured and calculated XRD patterns are presented in Fig. 6a. As listed in Table 2, the refined cell parameters are a = b = 5.2052 Å, c = 11.5470 Å, and α = 90° with a space group $I4_1/a$ (No. 88). The goodness of fit of refinement, which is defined as the ratio of R_{wp} to R_{exp}, is 1.87. A schematic of the crystal structure is shown in Fig. 6a. To further confirm the $CBMV_{0.34}$ structure, high-resolution transmission electron microscopy (HRTEM) and selected area electron diffraction (SAED) patterns analysis were employed. Fig. 6b, c display the HRTEM image and SAED patterns of $CBMV_{0.34}$ ceramic recorded along the [$\bar{1}$11] zone axis. The HRTEM image shows that the characteristic spacings of the (101) and (01$\bar{1}$) lattice planes of $CBMV_{0.34}$ ceramic are all 0.48 nm, which correspond well with XRD refinements. Fig. 6e illustrates the $CBMV_{0.34}$ crystal structure along the direction of the corresponding zone axes. The HRTEM image and schematic of crystal structure can be well matched, and the structural models of a $CBMV_{0.34}$ cell are superposed on the Fig. 6d (a partial enlargement of HRTEM). All these results are in good agreement, which fully demonstrates that $CBMV_{0.34}$ belongs to the tetragonal structure with a space group $I4_1/a$ (No. 88).

X-ray photoelectron spectroscopy (XPS) was performed for $CBMV_{0.34}$ ceramic to analyze chemical composition and oxidation state of each element. Fig. 7a–f illustrates the XPS spectra of $CBMV_{0.34}$ with

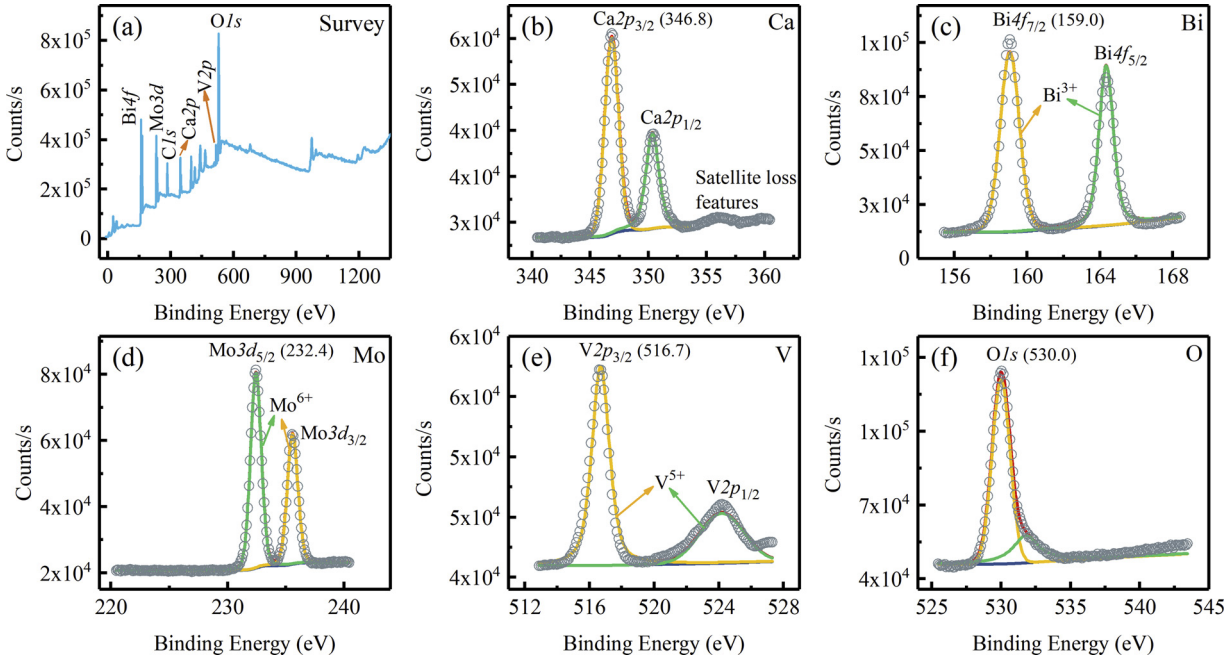

Fig. 7. XPS spectra of $CBMV_{0.34}$ ceramic with (a) the survey spectrum and high-resolution spectra of (b) Ca 2p, (c) Bi 4f, (d) Mo 3d, (e) V 2p and (f) O 1 s. (all peaks have been calibrated with respect to the C 1 s peak at 284.8 eV).

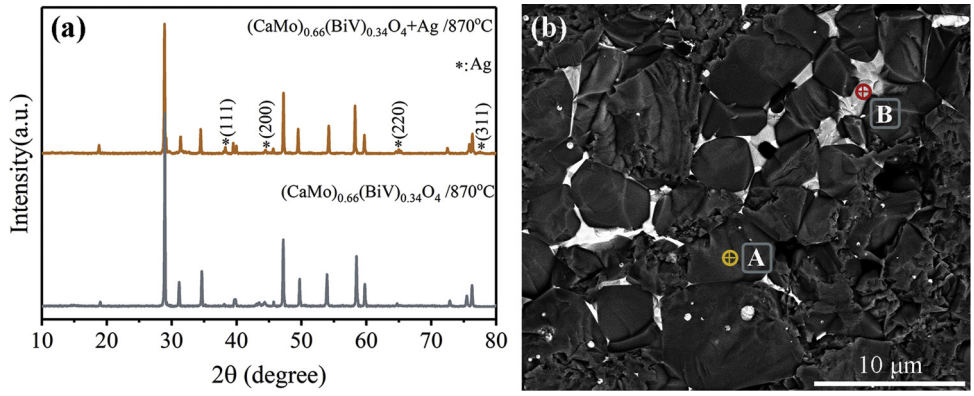

Fig. 8. X-ray diffraction patterns (a) and backscattered electron image (b) of the co-fired ceramic with 20 wt.% silver powders sintered at 870 °C.

the survey and high-resolution spectra of all elements. As shown in Fig. 7a, the survey spectrum revealed the presence of Ca, Bi, Mo, V, and O in $CBMV_{0.34}$ and C from contamination carbon as reference. The peak position also confirmed the oxidation state of each element as presented in Fig. 7b–f. The peak located at 530.0 eV is assigned to O 1 s of O^{2-} [34]. The Ca ($2p_{3/2}$) peak at 346.8 eV agreed with the peak position of $CaCO_3$ in the literature [35], and Bi ($4f_{7/2}$) at 159.0 eV and Mo ($3d_{5/2}$) at 232.4 eV matched well with $BiVO_4$ and $CoMoO_4$, respectively [36,37]. XPS signals from V 2p can be found at binding energies of 516.7 eV ($2p_{3/2}$) and 524.2 eV ($2p_{1/2}$), with a doublet splitting of 7.5 eV, consistent with the V 2p spin–orbit, which can be matched well with V_2O_5 [38]. These results confirmed that the oxidation states of Ca, Bi, Mo and V, are +2, +3, +6 and +5, respectively, which are comparable to those of $CBMV_{0.34}$ for Ca, Bi, Mo and V.

The sintering temperature of $CBMV_{0.34}$ (870 °C) is lower than the melting point of Ag (~ 961 °C), which raises the possibility that $CBMV_{0.34}$ ceramic may be suitable for LTCC technology, provided that no reaction occurs. To evaluate the chemical compatibility of $CBMV_{0.34}$ ceramic with silver electrode, it was co-fired with 20 wt.% Ag powders at 870 °C for 2 h. Fig. 8a–b shows the XRD pattern and backscattered electron images (BEI) of the co-fired ceramic. From the XRD results, it is seen that only the diffraction peaks of $CBMV_{0.34}$ and Ag were detected. Furthermore, we clearly observed in Fig. 8b that there are two types of grains, one with dark-color (marked as A) and the other with light-color (marked as B). EDS analysis was employed to identify the chemical compositions of two different color grains. According to the EDS analysis, the dark colored grains belong to $CBMV_{0.34}$ phase while the light colored grains belong to Ag phase. These results confirmed that the chemical compatibility between $CBMV_{0.34}$ ceramic and Ag electrodes, indicating that the $CBMV_{0.34}$ ceramic have potential for exploitation in LTCC technology.

4. Conclusions

In the $Ca_{1-x}Bi_xMo_{1-x}V_xO_4$ ($0.2 \le x \le 0.5$) ceramics, we found that a tetragonal scheelite structured solid solution was formed in the composition range $0.2 \le x \le 0.5$. As x increased from 0.2 to 0.5, sintering temperature of the $Ca_{1-x}Bi_xMo_{1-x}V_xO_4$ ceramics decreased from 880 to 800 °C, while the TCF shifted linearly from -44.9 to + 71.6 ppm/°C. Optimum microwave dielectric properties can be obtained in $Ca_{0.66}Bi_{0.34}Mo_{0.66}V_{0.34}O_4$ ceramic sintered at 870 °C for 4 h, with a ε_r ~ 21.9, a Qf ~ 18,150 GHz (at 7.2 GHz) and a TCF ~ + 0.1 ppm/°C. It is demonstrated that a temperature-stable microwave dielectric ceramics can be obtained by the substitution of (Bi, V) for (Ca, Mo) in $CaMoO_4$. Therefore, we conclude that the substitution of (Bi, V) for (Ca, Mo) is an effective way to adjust the TCF value of $CaMoO_4$ to near zero and to decrease the sintering temperature effectively. Furthermore, we found that the $Ca_{0.66}Bi_{0.34}Mo_{0.66}V_{0.34}O_4$ ceramic is chemically compatible with Ag powders at its sintering temperature, suggesting that this system could be good candidate for LTCC technology applications.

Acknowledgements

This work was supported by the National Key Research and Development Program of China (2017YFB0406301), the National Natural Science Foundation of China (U1632146), the Key Basic Research Program of Shaanxi Province (2017GY-129), and the Fundamental Research Funds for the Central University. The authors would like to thank the administrators in IR beamline workstation (BL01B) of National Synchrotron Radiation Laboratory (NSRL) for their help in the IR measurement and fitting. The SEM and TEM work was done at the International Center for Dielectric Research (ICDR), Xi'an Jiaotong University, Xi'an, China and the authors thank Ms. Yan-Zhu Dai and Mr Chuan-Sheng Ma for their help in using SEM and TEM. We thank Ms. Jiamei Liu at Instrument Analysis Center of Xi'an Jiaotong University for her assistance with XPS analysis.

References

[1] M.T. Sebastian, H. Jantunen, Low loss dielectric materials for LTCC applications: a review, Mater. Rev. 53 (2008) 57–90.
[2] D. Zhou, L.X. Pang, D.W. Wang, C. Li, B.B. Jin, I.M. Reaney, High permittivity and low loss microwave dielectrics suitable for 5G resonators and low temperature co-fired ceramic architecture, J. Mater. Chem. C 5 (2017) 10094–10098.
[3] D. Zhou, D. Guo, W.B. Li, L.X. Pang, X. Yao, D.W. Wang, I.M. Reaney, Novel temperature stable high-εr microwave dielectrics in the Bi_2O_3–TiO_2–V_2O_5 system, J. Mater. Chem. C 4 (2016) 5357–5362.
[4] L.J. Golonka, Technology and applications of low temperature cofired ceramic (LTCC) based sensors and microsystems, Bull. Pol. Acad.: Tech. 54 (2006) 221–231.
[5] Y. Chen, E. Li, S. Duan, S. Zhang, Low temperature sintering kinetics and microwave dielectric properties of $BaTi5O_{11}$ ceramic, ACS Sustainable Chem. Eng. 5 (2017) 10606–10613.
[6] N. Joseph, J. Varghese, T. Siponkoski, M. Teirikangas, M.T. Sebastian, H. Jantunen, Glass-free CuMoO4 ceramic with excellent dielectric and thermal properties for ultralow temperature cofired ceramic applications, ACS Sustainable Chem. Eng. 4 (2016) 5632–5639.
[7] J. Varghese, T. Siponkoski, M. Teirikangas, M.T. Sebastian, A. Uusimäki, H. Jantunen, Structural, dielectric, and thermal properties of Pb free molybdate based ultralow temperature glass, ACS Sustainable Chem. Eng. 4 (2016) 3897–3904.
[8] S. Sameera, P.P. Rao, S. Divya, A.K.V. Raj, Brilliant IR reflecting yellow colorants in rare earth double molybdate substituted $BiVO_4$ solid solutions for energy saving applications, ACS Sustainable Chem. Eng. 3 (2015) 1227–1233.
[9] L.X. Pang, D. Zhou, Modification of $NdNbO_4$ microwave dielectric ceramic by Bi substitutions, J. Am. Ceram. Soc. (2019), https://doi.org/10.1111/jace.16290.
[10] D. Zhou, L.X. Pang, J. Guo, Z.M. Qi, T. Shao, Q.P. Wang, H.D. Xie, X. Yao, C.A. Randall, Influence of Ce substitution for Bi in $BiVO_4$ and the impact on the phase evolution and microwave dielectric properties, Inorg. Chem. 53 (2014) 1048–1055.
[11] A.V. Veresnikova, B.K. Lubsandorzhiev, I.R. Barabanov, P. Grabmayr, D. Greiner, J. Jochum, M. Knapp, C. Oßwald, R.V. Poleshuk, F. Ritter, Fast scintillation light from $CaMoO_4$ crystals, Nucl. Instrum. Methods Phys. Res. 603 (2009) 529–531.
[12] Y. Yin, Y. Gao, Y. Sun, B. Zhou, L. Ma, X. Wu, X. Zhang, Synthesis and photoluminescent properties of $CaMoO_4$ nanostructures at room temperature, Mater. Lett. 64 (2010) 602–604.
[13] G.K. Choi, J.R. Kim, S.H. Yoon, K.S. Hong, Microwave dielectric properties of scheelite (A = Ca, Sr, Ba) and wolframite (A = Mg, Zn, Mn) $AMoO_4$ compounds, J.

Eur. Ceram. Soc. 27 (2007) 3063–3067.
[14] M. Valant, D. Suvorov, Chemical compatibility between silver electrodes and low-firing binary-oxide compounds: conceptual study, J. Am. Ceram. Soc. 83 (2000) 2721–2729.
[15] L.X. Pang, D. Zhou, W.G. Liu, Z.M. Qi, Z.X. Yue, Crystal structure and microwave dielectric behaviors of scheelite structured (1-x)$BiVO_4$ -x$La_{2/3}MoO_4$ ($0.0 \leq x \leq 1.0$) ceramics with ultra-low sintering temperature, J. Eur. Ceram. Soc. 38 (2018) 1535–1540.
[16] D. Zhou, W.G. Qu, C.A. Randall, L.X. Pang, H. Wang, X.G. Wu, J. Guo, G.Q. Zhang, L. Shui, Q.P. Wang, H.C. Liu, X. Yao, Ferroelastic phase transition compositional dependence for solid-solution $[(Li_{0.5}Bi_{0.5})_xBi_{1-x}][Mo_xV_{1-x}]O_4$ scheelite-structured microwave dielectric ceramics, Acta Mater. 59 (2011) 1502–1509.
[17] R.M. Hazen, J.W.E. Mariathasan, Bismuth Vanadate: a high-pressure, high-temperature crystallographic study of the ferroelastic-paraelastic transition, Science 216 (1982) 991–993.
[18] D. Zhou, L.X. Pang, H. Wang, J. Guo, X. Yao, C.A. Randall, Phase transition, Raman spectra, infrared spectra, band gap and microwave dielectric properties of low temperature firing $(Na_{0.5x}Bi_{1-0.5x})(Mo_xV_{1-x})O_4$ solid solution ceramics with scheelite structures, J. Mater. Chem. 21 (2011) 18412–18420.
[19] R.D. Shannon, Revised effective ionic radii and systematic studies of interatomic distances in halides and chalcogenides, Acta Crystallogr. 32 (1976) 751–767.
[20] J. Xu, Nano Measurer, 1.2.0, Fudan University: P.R.C., 2008.
[21] Materials Data, Inc., Livermore, CA, USA, https://materialsdata.com.
[22] J. Zhang, R.Z. Zuo, Sintering behavior, structural phase transition and microwave dielectric properties of La1-xZnxTiNbO6-$_{x/2}$ ceramics, J. Am. Ceram. Soc. 100 (2017) 4362–4368.
[23] Y. Lv, R.Z. Zuo, Microstructure and microwave dielectric properties of low-temperature sinterable (1-x)$Ba_3(VO_4)_2$-x$CaWO_4$ composite ceramics, J. Mater. Sci.: Mater. Electron. 24 (2013) 1225–1230.
[24] Y.H. Chen, H. Wang, L.X. Pang, H.F. Zhou, X. Yao, Effect of Zn^{2+} substitution on sintering behavior and dielectric properties of $NdNbO_4$ ceramics, Ferroelectrics 407 (2010) 61–68.
[25] D. Zhou, L. Pang, Z. Qi, Crystal structure and microwave dielectric behaviors of ultra-low-temperature fired x$(Ag_{0.5}Bi_{0.5})MoO_4$–(1–x)$BiVO_4$ ($0.0 \leq x \leq 1.0$) solid solution with scheelite structure, Inorg. Chem. 53 (2014) 9222–9227.
[26] D. Zhou, J. Li, L.X. Pang, D.W. Wang, I.M. Reaney, Novel water insoluble $(Na_xAg_{2-x})MoO_4$ ($0 \leq x \leq 2$) microwave dielectric ceramics with spinel structure sintered at 410 degrees, J. Mater. Chem. C 5 (2017) 6086–6091.
[27] R.S. Roth, J.L. Waring, Synthesis and stability of bismutotantalite, stibiotantalite and chemically similar ABO_4 compounds, Am. Mineral. 48 (1963) 1348–1356.
[28] G.K. Choi, S.Y. Cho, J.S. An, K.S. Hong, Microwave dielectric properties and sintering behaviors of scheelite compound $CaMoO_4$, J. Eur. Ceram. Soc. 26 (2006) 2011–2015.
[29] R.D. Shannon, R.A. Oswald, J.B. Parise, B.H.T. Chai, P. Byszewski, A. Pajaczkowska, R. Sobolewski, Dielectric constants and crystal structures of $CaYAlO_4$, $CaNdAlO_4$, and $SrLaAlO_4$, and deviations from the oxide additivity rule, J. Solid State Chem. 98 (1992) 90–98.
[30] R.D. Shannon, Dielectric polarizabilities of ions in oxides and fluorides, J. Appl. Phys. 73 (1993) 348–366.
[31] D. Zhou, H. Wang, Q.P. Wang, X.G. Wu, J. Guo, G.Q. Zhang, L. Shui, X. Yao, C.A. Randall, L.X. Pang, H.C. Liu, Microwave dielectric properties and Raman spectroscopy of scheelite solid solution $[(Li_{0.5}Bi_{0.5})_{1-x}Ca_x]MoO_4$ ceramics with ultra-low sintering temperatures, Funct. Mater. Lett. 3 (2010) 253–257.
[32] J.D. Bierlein, A.W. Sleight, Ferroelasticity in $BiVO_4$, Solid State Commun. 16 (1975) 69–70.
[33] S.P.S. Porto, J.F. Scott, Raman spectra of $CaWO_4$, $SrWO_4$, $CaMoO_4$, and $SrMoO_4$, Phys. Rev. 157 (1967) 716–719.
[34] B. Barbaray, J.P. Contour, G. Mouvier, Effects of nitrogen dioxide and water vapor on oxidation of sulfur dioxide over vanadium pentoxide particles, Environ. Sci. Technol. 12 (1978) 1294–1297.
[35] W.J. Landis, J.R. Martin, X-ray photoelectron spectroscopy applied to gold--decorated mineral standards of biological interest, J. Vac. Sci. Technol. A 2 (1984) 1108–1111.
[36] Y. Schuhl, M. Le Bras, J.-M. Leroy, J. Grimblot, Study of mixed-oxide catalysts containing bismuth, vanadium and antimony. Preparation, phase composition, spectroscopic characterization and catalytic oxidation of propene, J. Chem. Soc. Faraday Trans. 79 (1983) 2055–2069.
[37] A. Cimino, D. Angelis, The application of X-ray photoelectron spectroscopy to the study of molybdenum oxides and supported molybdenum oxide catalysts, J. Catal. 36 (1975) 11–22.
[38] T. Lindblad, B. Rebenstorf, Z.G. Yan, S.L.T. Andersson, Characterization of vanadia supported on amorphous $AlPO_4$ and its properties for oxidative dehydrogenation of propane, Appl. Catal. A Gen. 112 (1994) 187–208.